

Quantum effects in molecular dynamics with Many Interacting Worlds

Simone Sturniolo

Scientific Computing Department, STFC,

*Rutherford Appleton Laboratory, Harwell Campus, Didcot, OX11 0QX**

Abstract

While historically many quantum mechanical simulations of molecular dynamics have relied on the Born-Oppenheimer approximation to separate electronic and nuclear behavior, recently a lot of interest has arisen towards quantum effects in nuclear dynamics as well, especially protons. Due to the computational difficulty of solving the Schrödinger equation in full, though, these effects are often treated with approximated, quasi-classical methods.

In this paper we present an extension to the Many Interacting Worlds approach to quantum mechanics developed using a kernel method to rebuild the probability density. This approach, at a difference with the approximation presented in the original paper, can be naturally extended to n -dimensional systems, making it a viable method for approximating both ground states and quantum evolution of physical systems. The behavior of the algorithm is studied in different potentials and numbers of dimensions and compared both to the original approach and to exact Schrödinger equation solutions whenever possible.

* simone.sturniolo@stfc.ac.uk

CONTENTS

I. Introduction	2
II. The Many Interacting Worlds approach	3
III. Simulation details	6
IV. Results	8
A. Energy	8
B. Ground state convergence	10
C. Finite temperature effects	11
V. Conclusions and future prospects	13
Acknowledgments	14
A. Calculation of quantum forces with Gaussian and exponential kernels	14
B. Normalization of the exponential kernel	17
C. A matrix Numerov method for integration of the Schrödinger equation in arbitrary dimensions	18
References	20

I. INTRODUCTION

Since their original introduction [1] Ab-Initio Molecular Dynamics have been widely used to study a range of different systems. Historically, these simulations have always relied on the Born-Oppenheimer approximation [2] to separate between electronic and nuclear motions, treating the first with quantum mechanics and the latter with classical Newtonian mechanics. In recent years, however, an interest has arisen towards the relevance of quantum effects in nuclear motions, as advances in computational technology have made their calculation more practical. Many calculations and experiments suggest that quantum effects, especially involving the motion of hydrogen nuclei, may be in fact crucial for a full understanding of

water and ice [3, 4], strongly hydrogen bonded systems [5] and biological macromolecules [6]. Simulating these effects is no easy feat. One of the most popular approaches is Path-Integral Molecular Dynamics (from now on PIMD) [7], which allows one to approximate quantum statistical distributions by replacing a single nucleus with many copies of it organized as beads in a "ring polymer", all behaving classically except for a fictitious harmonic potential term linking them together.

In 2014, Hall, Deckert and Wiseman proposed a possible interpretation of quantum mechanics that shares many features with PIMD [8]. In this approach, that the authors call Many Interacting Worlds (MIW), quantum mechanical behavior emerges from many copies of the same particle all interacting with each other through a potential that has no classical equivalent. In addition, while generally PIMD works in imaginary time and can only compute quantum probability distributions, MIW is theoretically able to simulate time-dependent quantum evolution as well. While the theory presented in [8] is general, though, the practical implementation proposed in the paper can be applied only to 1-dimensional systems. In this paper we propose a different approach that is naturally extensible to higher dimensions and could therefore be put to practical use in molecular dynamics simulations.

II. THE MANY INTERACTING WORLDS APPROACH

The MIW approach, as presented in [8], can be considered as a discretization of the Holland-Poirier hydrodynamical approach to QM [9, 10] or it can be derived from the well known deBroglie-Bohm pilot wave interpretation [11, 12]. For the full derivation, we direct the reader to the original paper. Here we just give an outline of the fundamentals of this approach.

The system to be described is represented by a number of worlds N , with a multi-world configuration at time t

$$\mathbf{X}_t = \{\mathbf{x}_1(t), \mathbf{x}_2(t), \dots, \mathbf{x}_N(t)\} \quad (1)$$

with every $\mathbf{x}_n(t) = [x_{1,n}(t), x_{2,n}(t), \dots, x_{K,n}(t)]$ being the total classical configuration of world n ; namely, an array of the K degrees of freedom of the system. For a generic D -dimensional system containing P particles it will be $K = PD$. It is easy to see how then the probability density to find the system in a configuration \mathbf{q} , equivalent to the square modulus

of the wave function in the usual Schrödinger's picture, can be expressed as

$$P_t(\mathbf{q}) = |\Psi^2(\mathbf{q}, t)| = \sum_{n=1}^N \delta(\mathbf{q} - \mathbf{x}_n(t)) \quad (2)$$

using the Dirac delta distribution. The dynamics of the system are governed by the usual laws of Newtonian mechanics. The classical Hamiltonian can be written as:

$$\mathbb{H}_{MIW}(\mathbf{X}) = \sum_{n=1}^N \left[\sum_{k=1}^K \frac{1}{2} m_k \dot{x}_{k,n}^2 + V(\mathbf{x}_n) \right] + U_{MW}(\mathbf{X}) \quad (3)$$

where one can distinguish a term which operates on each world configuration separately (with the classical potential V also including any regular interactions among particles, like electrostatic forces) and an inter-world potential U_{MW} , which is non-classical in nature and introduces quantum effects. For example, delocalization is the consequence of U_{MW} being repulsive and preventing all particles to find an equilibrium in the potential minimum, and energy indeterminacy is the consequence of energy being exchanged between worlds thanks to the inter-world coupling and therefore not being conserved in each separate world (while the overall many-world ensemble is indeed conservative).

The general form of U_{MW} is:

$$U_{MW}(\mathbf{X}) = \sum_{n=1}^N \sum_{k=1}^K \frac{1}{2m_k} \left[g_N^k(\mathbf{x}_n; \mathbf{X}) \right]^2 \quad (4)$$

where

$$g_N^k(\mathbf{q}; \mathbf{X}) \approx \frac{\hbar}{2} \frac{1}{P(\mathbf{q}; \mathbf{X})} \frac{\partial P(\mathbf{q}; \mathbf{X})}{\partial q_k} \quad (5)$$

From Eq. 4 and 5 it is clear that to run a simulation based on the MIW approach it is necessary to rebuild the probability density function $P(\mathbf{q}; \mathbf{X})$ in some approximated way for a given multi world configuration. This is implied in the choice of only writing an "approximate" equality in Eq. 5. Eq. 2 suggests one way to do this, but it is obvious that in practical computation, where limits on available power and time will force one to use a small number of worlds N , this method would fail rather badly. In [8], the authors propose for the 1D case an approximation

$$P(x_n) \approx \frac{1}{N(x_{n+1} - x_n)} \quad (6)$$

which holds whenever the distance between the same particle in adjacent worlds is slowly varying and by enforcing that $x_{n+1} > x_n$ all the time, and does indeed produce good results. This leads to an inter-world potential depending overall on five worlds - the world of interest n and its first and second neighbors. It has however two problems that prevent it from being applicable to general purpose simulations, namely that it can not be naturally extended to more than one dimension and that it features a divergent potential which makes numerical integration very sensitive to the time step used when any two world-particles happen to be close enough.

In this paper we suggest a different method to compute the probability density which overcomes these problems. The idea is simply to apply a kernel distribution \mathcal{K} to Eq. 2, so that

$$P(\mathbf{q}) = \sum_{n=1}^N \mathcal{K}(\mathbf{q} - \mathbf{x}_n) \quad (7)$$

In this way, and with a good choice of function \mathcal{K} , $P(\mathbf{q})$ is continuous and derivable on all space, which leads to a natural way of computing the quantum forces, and can be defined similarly for any dimensionality. An obvious choice is to make the kernel function Gaussian, which, including the necessary normalization conditions, returns:

$$P(\mathbf{q}) = \frac{1}{N(\sqrt{\pi}b)^D} \sum_{n=1}^N \exp \left[-\frac{(\mathbf{q} - \mathbf{x}_n)^2}{b^2} \right] \quad (8)$$

with b a free kernel bandwidth parameter and D number of dimensions of the system. It is then possible to derive analytically the potential and the forces. While the process is not especially complex, the calculations are long, and are reported in Appendix A.

The Gaussian kernel however has the potential to give rise to a problem. Let us consider the case of a simulation of a single quantum particle. From now on, it must be clear that when we talk about "particles" we mean in fact multiple classical copies of the same particle across worlds interacting only through the quantum potential, and not effectively different particles interacting classically. Due to the appearance of the derivative of P in Eq. 5, one can see after deriving the forces that it will give rise to no repulsion when two particles are close enough or overlapping. This runs counter physical intuition: since the quantum potential must reproduce the effects of what we could call 'quantumness' on the system, it should be generally repulsive, to avoid the wave function collapsing in a single spot and

losing position indeterminacy. This is a property of any symmetric and smooth kernel, as its derivative in the center will always be null. Therefore, if the particles happened to get closer than a certain distance during the simulation, they might end up coalescing and this artifact would compromise the final result. For this reason we test also a different kernel, with a discontinuous, non-zero derivative in the origin:

$$P(\mathbf{q}) = \frac{\Gamma(D/2)}{2N(D-1)!(\sqrt{\pi}b)^D} \sum_{n=1}^N \exp\left[-\frac{|\mathbf{q} - \mathbf{x}_n|}{b}\right] \quad (9)$$

where the proper normalization factor has been inserted in front (with Γ meaning the gamma function). Since this factor is less obvious, proof of how it's derived is provided in Appendix B. Figure 1 compares the U_{MW} for two particles as the distance between them varies for both kernels and highlights the problem and the way the exponential kernel solves it. Potential and forces can be found for this kernel similarly to what has been seen with the Gaussian one, and are written out in Appendix A as well.

We will now proceed to test this method in some numerical simulations on toy models and compare its results with both solutions obtained by traditional methods based on diagonalization of the Hamiltonian and, for the case of 1D problems, MIW simulations carried out with the potential derived from Eq. 6.

III. SIMULATION DETAILS

Numerical simulations were carried out on a personal computer using Python and the scientific libraries Numpy and Scipy for matrix diagonalizations and optimization operations [13, 14]. The exact solution results in 1D were obtained by building an Hamiltonian based on a matrix Numerov method [15]. This approach was then expanded to higher dimensionality; the details are explained in Appendix C. Since this method uses a direct space basis set which enforces the condition $\psi = 0$ outside of the finite spatial grid, all potentials are treated effectively as if they were enclosed in an infinite potential well.

For the MIW method, the equations of motion were integrated using a standard velocity Verlet algorithm, and a Langevin thermostat was used for thermalization when required. In addition, an adaptive time step has been used, where at any given step i :

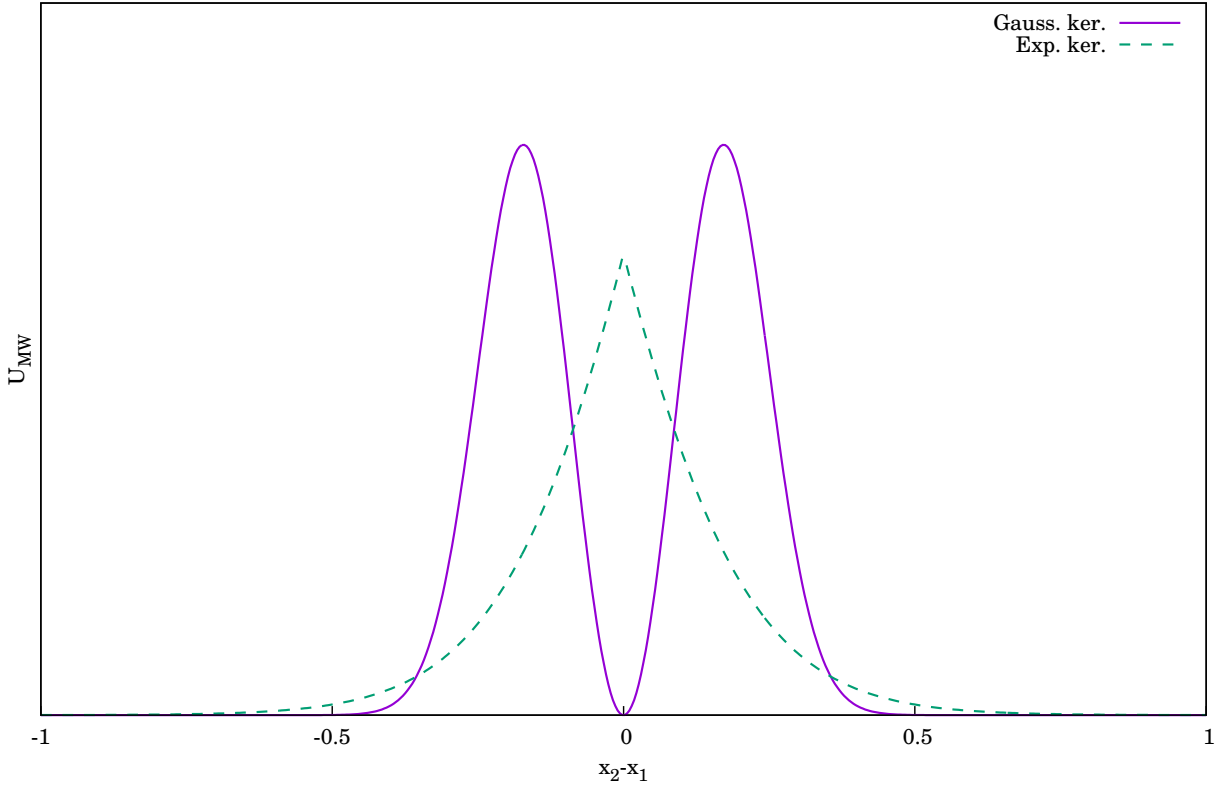


FIG. 1. Many world potential for $N = 2$ and for the cases of Gaussian and exponential kernels. It can be seen how the former features a minimum for the case of overlapping particles where the latter has a cusp. Units are arbitrary.

$$dt_i = \min \left(dt_0 \frac{\max(|F_0|)}{\max(|F_i|)}, dt_{\max} \right) \quad (10)$$

so that dt scales with the maximum force present in the system.

Particular attention, of course, must be paid to the initial estimate of the bandwidth parameter, b , which controls the radius of the interaction. This is a common problem in kernel density estimation, well known in statistics. Given the particle positions, one has to find the kernel width that best fits the target probability distribution. For cases where the initial desired probability distribution is known (for example, when initialising a simulation with knowledge of the ground state), the AMISE method was used. For those where instead only an educated guess was possible, the Silverman method was employed. Both these methods are described in [16].

IV. RESULTS

A. Energy

In these tests we focus on the performance of the MIW approach in dealing with the ground state of a proton in a few example potentials. We initialise the MIW system by using the known ground state probability density obtained from diagonalising the Hamiltonian and consider the error in the energy so obtained, in order to compare the different kernels and dimensionalities in ideal conditions.

The potentials used are of two types. One is a simple harmonic potential of the form

$$V_{harm}(\mathbf{x}) = \frac{k}{2}\mathbf{x}^2 \quad (11)$$

while the other is a multi-dimensional Lennard-Jones potential with an angular term of the form

$$V_{lj}(\mathbf{x}) = \Delta V_r \left[\left(\frac{|\mathbf{x} - \mathbf{x}_0|}{r_0} \right)^{-12} - 2 \left(\frac{|\mathbf{x} - \mathbf{x}_0|}{r_0} \right)^{-6} \right] + \Delta V_\alpha \left(1 - \frac{\mathbf{x} - \mathbf{x}_0}{|\mathbf{x} - \mathbf{x}_0|} \cdot \hat{i} \right) \quad (12)$$

where \hat{i} is the versor of the x-axis. This was chosen to represent a crude approximation of a chemical bond. In this part we use three such potentials, which from now on we will label `harm1`, `harm10` and `lj1`. The first two are defined by Equation 11 with $k = 1$ and $k = 10 \text{ eV}/\text{\AA}^2$ respectively. The third uses Equation 12 with $\Delta V_r = 1 \text{ eV}$, $\mathbf{x}_0 = -2.5\hat{i} \text{ \AA}$, $r_0 = 1 \text{ \AA}$ and $\Delta V_\alpha = 10 \text{ eV}$. It should be noted that the origin for the LJ potential was chosen because all simulations were ran in box-shaped grids ranging from -2 to 2 \AA . The grids had 200, 40 and 15 points of side respectively for 1, 2 and 3D. The wave function is considered zero outside of this space. Thus, this choice allows to have the minimum of the potential inside the box without including the singularity, which could cause problems.

The initial particle positions were generated in two different ways. The first method was to distribute the particles so that each grid element contains just the right amount to match the target distribution as closely as possible. The second instead employed a simple Monte Carlo method to randomly distribute them, following the target distribution but allowing for random fluctuations.

When calculating the energy within the MIW approximation in order to compare it to the energy found by diagonalising the Hamiltonian, care needs to be taken. In the basic

approach, forces are calculated on the hypothesis of perfectly point-like particles, and would in fact be exact for an infinite number of particles with infinitesimally small spacing. When using kernels, each particle contributes to the overall density with a distributed density. This can be interpreted as each particle representing, in fact, a large or infinite number of particles distributed according to that function and moving around rigidly. This brings forth two main consequences for energy calculations:

- the i -th particle's contribution to potential energy, V_i , should in theory not be calculated in a pointlike manner, $V(x_i)$, but rather as the integral

$$V_i = \int_{\mathbb{R}^D} V(\mathbf{x}) \mathcal{K}(\mathbf{x}) d\mathbf{x} \quad (13)$$

This might not always be possible in actual calculations. In that case, the point-like approximation is accurate to the first order, since the kernel is symmetric. If one has access to the second derivative of the potential it is possible to expand it in Taylor series and find a third order approximation which also depends on b ;

- there is an "internal energy" correction for each particle, consisting of the many world interaction energy of the particles constituting the Gaussian distribution kernel itself. This is a constant term and can be calculated by applying Equation 4, replacing the probability density in Eq. 5 with the kernel function and the sum over n with an integral over all space. Luckily, it is rather easy to calculate for both kernels:

$$U_{corr}^{(gauss)} = \frac{\hbar^2}{4m} \frac{D}{b^2} \quad U_{corr}^{(exp)} = \frac{\hbar^2}{8m} \frac{D}{b^2} \quad (14)$$

It should be remarked that this term is not required when comparing two MIW simulations with the same parameters, being constant; it becomes necessary however if considering simulations of different kind or with different b .

Figure 2 shows the error in energy calculated with the MIW approach for the various potentials and dimensionalities tested. A few observations are in order. Convergence is overall satisfactory in all cases, with various degrees of success. The 1D case shows obviously the advantages of the kernel approximation compared to the one given in Equation 6. Whereas the kernel approximation converges indefinitely to the exact energy as the number of worlds increases, both with Gaussian and exponential kernels, the simpler method converges only

initially to then immediately diverge when the density of the worlds becomes too high, as its dependency on the inverse of the distance between world-particles makes it far more sensitive to numerical errors. This is even more obvious for Monte-Carlo generated particle configurations, which fall outside of the range of the plot altogether.

In the 2D and 3D cases, random Monte-Carlo initialization provides a better average approximation but also greater noise, whereas uniform distributions quickly converge to a slightly biased value. This is probably the effect of such distributions being dependent on the underlying grid, which introduces artefacts. Still, the energy seems to be reliably reproduced, with the biggest deviations being observed in the 3D `harm10` case. This is caused by the interaction of such a steeply varying potential with the very coarse 3D grid.

B. Ground state convergence

Now we move on to investigating a method of finding the ground state of a potential by using the MIW approach. This is straightforward: we generate a system of a number of worlds (in all cases here, $N = 50$ was used) in some configuration that we consider a reasonable starting point, then we carry out a strongly damped classical dynamics calculation whereas we relax this system to its energy minimum. In addition to that, since it's possible that particles might get stuck in unphysical configurations or local minima, the simulation is periodically re-initialized by computing the density and using it to re-distribute the particles. This was done using the uniform distribution method, which is found to give the better results. For all these simulations, 10 sequences of 1000 time steps, with $dt_{max} = 5 \cdot 10^{-17} s$ ($3 \cdot 10^{-17} s$ for the 3D case) were used, with one re-initialization between each sequence. Damping was achieved by using a Langevin thermostat with $T = 0 K$ and $\gamma = 10^{15} s^{-1}$. The initial configuration was chosen to be a completely uniform distribution for the harmonic potentials and a Gaussian centred on the minimum for the Lennard-Jones ones. This choice was made because the latter, being much flatter on the long distance, risked causing convergence problems to an ensemble of particles that is too spread out. This was not considered a problem as it seems reasonable to expect that in all practical applications similar assumptions could be made.

The results of the calculation can be seen in Figures 3 and 4, for convergence of energy

over time and the root sum square (RSS) of the probability density error on the grid, that we label as χ , at the end of each iteration of 1000 steps. The energy error clearly displays dents corresponding to each reinitialization, but after the first few iterations it generally falls back to its converged value. As a general rule, one can see the exponential kernel performing generally slightly better, except for the `1j1` 2D case, where the energy seems to diverge. Again, the grid obviously plays a role - the most egregious failure being evident in the χ value for the 3D `harm1` potential. Here the energy in fact is approximated well, but there is a huge deviation in the density, caused by the fact that the grid spacing is big compared to the width of the distribution itself and thus errors are amplified.

In general, this method appears to be promising but sensitive to the choices of parameters made. Periodically reinitializing the configuration or other corrective approaches can be used to prevent it from developing artifacts.

C. Finite temperature effects

We now move on to examining a simple example of possible application of MIW simulations to the realm of finite temperature quantum dynamics. While the original MIW theory does not explicitly mention temperature, there is no reason to think that it should not be possible to simulate incoherent finite temperature quantum dynamics by simply plugging one of the well known MD thermostats into a MIW simulation. This is a consequence of the fact that thermostats approximate the system's interaction with the environment, and classical interactions between different particles in a MIW simulation are perfectly equivalent to the ones in a regular simulation. An interesting question is whether the thermostats should be correlated or coupled across worlds. Intuitively, correlated thermostats would represent an environment that is concentrated in a relatively small region of the phase space and evolves coherently in time, whereas uncorrelated thermostats would represent an environment widely dispersed in phase space and decohered. While there may be some interesting insights to be gained from exploring this matter, for the time being we will settle for fully uncorrelated thermostats, that seem to paint a much more realistic portrait of the situation, especially for high temperatures.

Figure 5 gives us a simple insight in how MIW simulations can reproduce thermal effects.

The full bundle of trajectories, from starting configuration to the end of a molecular dynamics simulation, are shown for three different temperatures. The 0 K case is a perfect example of a damped MIW system converging to its ground state, with the contraction (driven by the external potential) being eventually countered by the repulsion due to the MIW potential, finding an equilibrium. By comparison, the higher temperatures tell a different story; the trajectories get scrambled and the system expands. The collisions may transfer further energy among particles so that fluctuations will be wilder than they would be in a non-interacting ensemble, and may allow particles to overcome barriers that should be impassable (thus allowing tunnelling). Ultimately, when the temperature is high enough, the MIW potential's contribution becomes tiny compared to the thermostat forces, and the system reaches the classical limit.

The system chosen for testing whether the MIW approach can reproduce temperature-dependent quantum tunnelling rates is a simple double well built by joining two harmonic potentials along a plane, as seen in Figure 6. This system has been studied by Bell [17] and its tunnelling rate temperature dependence is known. We choose a potential formed by two harmonic wells of $k = 10\text{ eV}/\text{\AA}^2$ with $x_0 = 0.2\text{ \AA}$. This leads to a potential barrier of $\Delta E = kx_0^2/2 = 0.2\text{ eV}$ and turning points situated at $a \sim 0.06\text{ \AA}$. The Arrhenius classical jumping rate is:

$$\nu_c = \nu_0 \exp\left(-\frac{\Delta E}{k_B T}\right) \quad (15)$$

whereas the Bell quantum corrected version is

$$\nu_q = \nu_0 \frac{1}{\beta - \frac{\Delta E}{k_B T}} \left[\beta \exp\left(-\frac{\Delta E}{k_B T}\right) - \frac{\Delta E}{k_B T} \exp(-\beta) \right] \quad (16)$$

with

$$\beta = \frac{a\pi\sqrt{2m\Delta E}}{\hbar} \sim 1.77 \quad (17)$$

Three separate simulations were run with $N = 50$ worlds: one with a Gaussian kernel, one with an exponential kernel, and one with no kernel forces at all, making it effectively 50 decoupled classical simulations. A Langevin thermostat with $\gamma = 10^{14}\text{ s}^{-1}$ was used. Here a little digression is in order. It is common wisdom that Langevin thermostats should not be used when computing diffusion rates; however, there's reason to believe this is justified

in this specific case. The rationale for not using it in ordinary MD simulations is that a Langevin thermostat fully couples each individual particle to the heat bath, and this is unrealistic for, for example, molecules in a fluid. However this is not the case here: we are effectively simulating only one particle, and each copy we do simulate is in fact fully coupled, classically, to its own heat bath, namely, the rest of its world. There is no doubt, of course, that the chosen γ will control the time scale of the process (in fact, it seems hardly a coincidence that as seen latter we will find $\nu_0 = \gamma$). However, since we are interested in comparing jumping rates, and how the MIW potential enhances them, rather than in their absolute values, this is not necessarily a problem. For multi-particle simulations of course the usual considerations would apply, and a Nosé-Hoover thermostat would be more suited to the task at hand.

Tunnelling was calculated by measuring the fraction of the density inside the starting well and fitting an exponential decay curve to it as it fell from its initial value of almost 1 (some leakage due to the tails of the distributions is present) to the equilibrium value of 0.5. The no kernel simulation was used as benchmark to fit the value of ν_0 , using Equation 15, which was then plugged into Equation 16 to estimate the quantum jumping rate.

Figure 7 shows the final result. The Arrhenius model was fitted with $\nu_0 = 10^{14} s^{-1}$, and the result applied to the Bell model. The rates originated from the exponential kernel simulations follow it closely, showing that the quantum MIW potential does indeed enhance the jumping process and reproduce the correct tunnelling dynamics. The Gaussian kernel simulations behave closer to the ones without kernel at the beginning and then catch up with the quantum model around $T = 750 K$. This is probably due to the already mentioned issue with particles ‘bonding’ when using a smooth kernel, and the problem is overcome once the system has enough kinetic energy to break those pairs. The calculation suggests that it is indeed possible to simulate finite temperature quantum dynamical effects with the MIW method.

V. CONCLUSIONS AND FUTURE PROSPECTS

An extension to the Many Interacting Worlds description of QM first introduced in [8] that makes use of kernel density estimation has been proposed. The method appears to give promising results in reproducing the solutions of simple quantum problems with an

ensemble of coupled classical simulations and opens up a novel road to real time finite temperature quantum dynamics for ab-initio molecular dynamics and the study of quantum nuclear effects.

Some details of the method need to be better understood before applying it to molecular dynamics problems. For example, the Gaussian kernel has been shown to often perform worse than the exponential one due to its smoothness; however, the same quality makes it ideal to approximate the true density distribution. A way to overcome the smoothness problem would be desirable. A possible road would be to make the kernel width b a dynamical variable, allowing kernels to squeeze when two particles come too close so that their repulsion grows and they never get to the point of overlapping. This would make the calculations more complex but would also add more degrees of freedom to the system and possibly make it better at approximating the true wave function. A recent work [18] also suggests a connection between the choice made for probability density reconstruction and which quantum state the particles effectively approximate. The logic is hard to translate to the kernel method used here, but if possible it might shed some light on a way to simulate excited states specifically. Finally, the analogies between the MIW and the PIMD methods are striking and suggest that a deeper connection between the two might exist. Studying that might bring new insights on how to mitigate each method’s weaknesses by mixing it with the other.

ACKNOWLEDGMENTS

Thanks for the useful discussions to Phil Hasnip, Leonardo Bernasconi and Dominik Jochym. This work was conducted within the framework of the CCP for NMR crystallography, which is funded by the EPSRC grants EP/J010510/1 and EP/M022501/1.

Appendix A: Calculation of quantum forces with Gaussian and exponential kernels

We now show how equation 4 and its derivatives can be computed efficiently assuming the probability is constructed with a Gaussian kernel, as seen in 7. This formalism is designed to make for especially compact code when working with languages that allow for element-wise array operations like Fortran or Python+Numpy. Let us consider the case of a single quantum particle represented with N worlds in D dimensions. The coordinate of

the particle in world i along dimension k is written as $x_i^{(k)}$. Let us also consider a kernel of fixed bandwidth b . Then we define:

$$\begin{aligned} r_{ij}^{(k)} &= x_i^{(k)} - x_j^{(k)} & r_{ij}^2 &= \sum_k (r_{ij}^{(k)})^2 & P_{ij} &= \frac{1}{N(\sqrt{\pi}b)^D} \exp\left(-\frac{r_{ij}^2}{b^2}\right) \\ P_{ij}^{(k)} &= -\frac{2}{b^2} r_{ij}^{(k)} P_{ij} & P_{ij}'' &= -\frac{2}{b^2} \left(1 - \frac{2}{b^2} r_{ij}^2\right) P_{ij} \end{aligned} \quad (\text{A1})$$

In this formalism, P_{ij} represents the contribution of particle j to the density probability at the position of particle i , P_{ij}' its gradient with respect to the position of particle i , and so on. It should be noted that, while we included the normalisation factor in Eq. A1, this is not really relevant for the final forces as it disappears in the formulation of U_{MW} , which contains a ratio between the kernel and its derivative.

Computing the total quantities, summed over all particles, requires a bit more care. If we define:

$$P_i = \sum_j P_{ij} \quad (\text{A2})$$

as the total density probability at the position of particle i , then its derivatives are:

$$\frac{dP_i}{dx_n^{(l)}} = \begin{cases} P_n^{(l)} & n = i \\ -P_{in}^{(l)} & n \neq i \end{cases} \quad (\text{A3})$$

and the second ones:

$$\frac{dP_i^{(k)}}{dx_n^{(l)}} = \begin{cases} P_n''^{(l)} & n = i, l = k \\ -P_{in}''^{(l)} & n \neq i, l = k \\ -\frac{2}{b^2} \sum_j r_{nj}^{(k)} P_{nj}^{(l)} & n = i, l \neq k \\ \frac{2}{b^2} r_{in}^{(k)} P_{in}^{(l)} & n \neq i, l \neq k \end{cases} \quad (\text{A4})$$

where the quantities with only one index (P_n' , P_n'') represent sums over j as seen in Eq. A2. Using these relationships, it's straightforward, if rather tedious, to compute the quantum potential and the forces. We can rewrite eq. 4 for this kernel using the new formalism:

$$g_i^{(k)} = \frac{\hbar}{2} \frac{P_i'^{(k)}}{P_i} \quad U = \frac{1}{2m} \sum_{i,k} [g_i^{(k)}]^2 \quad (\text{A5})$$

Then the full derivative with respect to the particle positions can be written as:

$$\begin{aligned} \frac{dU}{dx_n^{(l)}} = & 2g_n^{(l)} \left[-\frac{1}{P_n^2} (P_n'^{(l)})^2 + \frac{1}{P_n} P_n''^{(l)} \right] + \\ & \sum_{i \neq n} 2g_i^{(l)} \left[\frac{1}{P_i^2} P_{in}'^{(l)} P_i'^{(l)} - \frac{1}{P_i} P_{in}''^{(l)} \right] + \\ & \sum_{k \neq l} 2g_n^{(k)} \left[-\frac{1}{P_n^2} P_n'^{(k)} P_n'^{(l)} - \frac{2}{b^2 P_n} \sum_j r_{nj}^{(k)} P_{nj}'^{(l)} \right] + \\ & \sum_{i \neq n, k \neq l} 2g_i^{(k)} \left[\frac{1}{P_i^2} P_{in}'^{(k)} P_i'^{(l)} + \frac{2}{b^2 P_i} r_{in}^{(k)} P_{in}'^{(l)} \right] \end{aligned} \quad (\text{A6})$$

where it should be noted that the two bottom summation terms are always going to be zero in the 1-dimensional case, which therefore noticeably simplifies the expression. The forces of course are going to be equal to this expression with a minus sign.

Now we consider the case of an exponential kernel. A lot of the passages are similar, but we need to take into account the different form of the derivatives. In this case we have:

$$\begin{aligned} r_{ij} &= \sqrt{\sum_k (r_{ij}^{(k)})^2} & P_{ij} &= \frac{\Gamma(D/2)}{2N(D-1)!(\sqrt{\pi}b)^D} \exp\left(-\frac{r_{ij}}{b}\right) \\ P_{ij}'^{(k)} &= -\frac{1}{b} \frac{r_{ij}^{(k)}}{r_{ij}} P_{ij} & P_{ij}'' &= -\frac{1}{b} \frac{1}{r_{ij}} \left[1 - \frac{(r_{ij}^{(k)})^2}{r_{ij}^2} - \frac{1}{b} \frac{(r_{ij}^{(k)})^2}{r_{ij}} \right] P_{ij} \end{aligned} \quad (\text{A7})$$

With these new assignments, Eq. A3 still holds for first derivatives, whereas second derivatives become:

$$\frac{dP_i'^{(k)}}{dx_n^{(l)}} = \begin{cases} P_n''^{(l)} & n = i, l = k \\ -P_{in}''^{(l)} & n \neq i, l = k \\ -\sum_j \frac{r_{nj}^{(k)}}{r_{nj}} \left(\frac{1}{r_{nj}} + \frac{1}{b} \right) P_{nj}'^{(l)} & n = i, l \neq k \\ \frac{r_{in}^{(k)}}{r_{in}} \left(\frac{1}{r_{in}} + \frac{1}{b} \right) P_{in}'^{(l)} & n \neq i, l \neq k \end{cases} \quad (\text{A8})$$

and therefore the forces:

$$\begin{aligned}
\frac{dU}{dx_n^{(l)}} = & 2g_n^{(l)} \left[-\frac{1}{P_n^2} (P_n'^{(l)})^2 + \frac{1}{P_n} P_n''^{(l)} \right] + \\
& \sum_{i \neq n} 2g_i^{(l)} \left[\frac{1}{P_i^2} P_{in}'^{(l)} P_i'^{(l)} - \frac{1}{P_i} P_{in}''^{(l)} \right] + \\
& \sum_{k \neq l} 2g_n^{(k)} \left[-\frac{1}{P_n^2} P_n'^{(k)} P_n'^{(l)} - \frac{1}{P_n} \sum_j \frac{r_{nj}^{(k)}}{r_{nj}} \left(\frac{1}{r_{nj}} + \frac{1}{b} \right) P_{nj}'^{(l)} \right] + \\
& \sum_{i \neq n, k \neq l} 2g_i^{(k)} \left[\frac{1}{P_i^2} P_{in}'^{(k)} P_i'^{(l)} + \frac{1}{P_i} \frac{r_{in}^{(k)}}{r_{in}} \left(\frac{1}{r_{in}} + \frac{1}{b} \right) P_{in}'^{(l)} \right]
\end{aligned} \tag{A9}$$

Appendix B: Normalization of the exponential kernel

The multivariate exponential kernel centered in the origin is defined as:

$$\mathcal{K}(\mathbf{q}) = \exp \left[-\frac{|\mathbf{q}|}{b} \right] \tag{B1}$$

for a given width b .

This needs to be divided by its integral over the entire space for normalization purposes. For the 1D case the solution is simple, as the integral

$$\int_0^\infty \exp \left(-\frac{x}{b} \right) dx = b \tag{B2}$$

is easily found, and thus the overall integral is $2b$. However the multivariate case is more complex. One can find it considering two things. First, the integral of a radial function in a D -dimensional space can be defined as

$$\int_{\mathbb{R}^n} f(|\mathbf{q}|) d\mathbf{q} = \int_0^\infty f(r) \omega_{D-1}(r) dr \tag{B3}$$

where ω_{D-1} is the surface area of the D -dimensional sphere [19]. This is known to be

$$\omega_{D-1}(r) = \frac{2\pi^{\frac{D}{2}}}{\Gamma\left(\frac{D}{2}\right)} r^{D-1} \tag{B4}$$

On the other hand, the radial integral can be carried out by parts if we notice that

$$\int_0^\infty \exp\left(-\frac{r}{b}\right) r^{D-1} dr = \left| -b \exp\left(-\frac{r}{b}\right) r^{D-1} \right|_0^\infty \quad (B5)$$

$$+ (D-1)b \int_0^\infty \exp\left(-\frac{r}{b}\right) r^{D-2} dr \quad (B6)$$

$$= (D-1)b \int_0^\infty \exp\left(-\frac{r}{b}\right) r^{D-2} dr \quad (B7)$$

as the first term goes to zero both on $r = 0$ and $r = \infty$. We can repeat the operation $D - 1$ times, thus finding:

$$\int_0^\infty \exp\left(-\frac{r}{b}\right) r^{D-1} dr = (D-1)!b^D \quad (B8)$$

which combined to the prefactor for the surface area of an n -sphere gives us

$$\int_{\mathbb{R}^D} \mathcal{K}(\mathbf{q}) = \frac{2(\sqrt{\pi}b)^D}{\Gamma\left(\frac{D}{2}\right)} (D-1)! \quad (B9)$$

whose reciprocal is the normalization factor we need.

Appendix C: A matrix Numerov method for integration of the Schrödinger equation in arbitrary dimensions

The original 1D matrix Numerov method for integrating the Schrödinger equation was presented in [15]. An analogue scheme for the 2D equation is described in [20]. Here we write the same scheme in a general form for any number of dimensions.

Similarly to what happens in 1D, the Numerov method is designed to solve equations of the form

$$\nabla^2 \psi(\mathbf{x}) = f(\mathbf{x})\psi(\mathbf{x}) \quad (C1)$$

where, in the case of the Schrödinger equation,

$$f(\mathbf{x}) = -\frac{2m}{\hbar^2}(E - V(\mathbf{x})) \quad (C2)$$

Now we expand ψ in a Taylor series, define the function on a grid, and consider the ‘stencil’ surrounding a grid point composed by all nearest neighbors - the points that are one step forward or backward in each direction. Then we can write

$$\sum_i^D \frac{\psi(\mathbf{x} + h_i \boldsymbol{\epsilon}_i) - 2\psi(\mathbf{x}) + \psi(\mathbf{x} - h_i \boldsymbol{\epsilon}_i)}{h_i^2} = f\psi + \frac{1}{12} \sum_i^D \frac{\partial^4 \psi}{\partial x_i^4} h_i^2 + \mathcal{O}(h^6) \quad (\text{C3})$$

with $\boldsymbol{\epsilon}_i$ unit vector and h_i grid step for dimension i . In this case the relation holds

$$\nabla^2(f\psi) = \nabla^2(\nabla^2\psi) = \sum_i^D \frac{\partial^4 \psi}{\partial x_i^4} + \sum_i^D \sum_{j \neq i}^D \frac{\partial^4 \psi}{\partial x_i^2 \partial x_j^2} \quad (\text{C4})$$

so we can separate

$$\begin{aligned} \sum_i^D \frac{\psi(\mathbf{x} + h_i \boldsymbol{\epsilon}_i) - 2\psi(\mathbf{x}) + \psi(\mathbf{x} - h_i \boldsymbol{\epsilon}_i)}{h_i^2} &= f\psi + \frac{1}{12} \sum_i^D \frac{\partial^2(f\psi)}{\partial x_i^2} h_i^2 \\ &\quad - \frac{1}{12} \sum_i^D h_i^2 \sum_{j \neq i}^D \frac{\partial^4 \psi}{\partial x_i^2 \partial x_j^2} \end{aligned} \quad (\text{C5})$$

Now, considering that we are working within a grid of finite size, we can write all operators as matrices. The matrix \mathbf{A} as described in [15] extends to a Kronecker sum:

$$\mathbf{A}^{(D)} = \sum_i^D \mathbf{A}_i^{(D)} = \bigoplus_i^D \frac{(\mathbb{I}_{-1} - 2\mathbb{I}_0 + \mathbb{I}_1)}{h_i^2} \quad (\text{C6})$$

while the matrix \mathbf{B} , which operates on $f\psi$ on the right-hand side, becomes:

$$\mathbf{B}^{(D)} = \mathbb{I} + \frac{1}{12} \sum_i^D h_i^2 \mathbf{A}_i^{(D)} \quad (\text{C7})$$

We can also write the mixed derivatives as matrix products

$$\frac{\partial^4}{\partial x_i^2 \partial x_j^2} \rightarrow \mathbf{A}_i^{(D)} \mathbf{A}_j^{(D)} \quad (\text{C8})$$

which happen to commute since the \mathbf{A} matrices are symmetric. So in the end we can write the multi-dimensional equivalent of the 1D Numerov method as:

$$\begin{aligned} -\frac{\hbar^2}{2m} \left[\mathbf{A}^{(D)} + \frac{1}{12} \sum_{i,j>i} \mathbf{A}_i^{(D)} \mathbf{A}_j^{(D)} (h_i^2 + h_j^2) \right] \psi &= \mathbf{B}^{(D)} (E - \mathbf{V}) \psi \implies \\ -\frac{\hbar^2}{2m} \mathbf{B}^{-1(D)} \left[\mathbf{A}^{(D)} + \frac{1}{12} \sum_{i,j>i} \mathbf{A}_i^{(D)} \mathbf{A}_j^{(D)} (h_i^2 + h_j^2) \right] \psi + \mathbf{V} \psi &= E \psi \end{aligned} \quad (\text{C9})$$

with \mathbf{V} a matrix having the potential along its diagonal and zero everywhere else. Therefore, this becomes an eigenvalue problem that can be solved by diagonalizing the matrix:

$$\mathbf{M} = -\frac{\hbar^2}{2m} \mathbf{B}^{-1(D)} \left[\mathbf{A}^{(D)} + \frac{1}{12} \sum_{i,j>i} \mathbf{A}_i^{(D)} \mathbf{A}_j^{(D)} (h_i^2 + h_j^2) \right] + \mathbf{V} \quad (\text{C10})$$

and will give us energies and eigenstates as a result.

[1] R. Car and M. Parrinello, “Unified approach for molecular dynamics and density-functional theory,” *Phys. Rev. Lett.*, vol. 55, pp. 2471–2474, 1985.

[2] M. Born and R. Oppenheimer, “Zur quantentheorie der molekeln,” *Annalen der Physik*, vol. 389, no. 20, pp. 457–484, 1927.

[3] X.-Z. Li, M. I. J. Probert, A. Alavi, and A. Michaelides, “Quantum nature of the proton in water-hydroxyl overlayers on metal surfaces,” *Phys. Rev. Lett.*, vol. 104, p. 066102, Feb 2010.

[4] B. Pamuk, J. M. Soler, R. Ramírez, C. P. Herrero, P. W. Stephens, P. B. Allen, and M.-V. Fernández-Serra, “Anomalous nuclear quantum effects in ice,” *Phys. Rev. Lett.*, vol. 108, p. 193003, May 2012.

[5] K. T. Wikfeldt, “Nuclear quantum effects in a 1-d model of hydrogen bonded ferroelectrics,” *Journal of Physics: Conference Series*, vol. 571, no. 1, p. 012012, 2014.

[6] Z. D. Nagel and J. P. Klinman, “Tunneling and dynamics in enzymatic hydride transfer,” *Chemical Reviews*, vol. 106, no. 8, pp. 3095–3118, 2006. PMID: 16895320.

[7] D. Marx and M. Parrinello, “Ab initio path-integral molecular dynamics,” *Zeitschrift für Physik B Condensed Matter*, vol. 95, no. 2, pp. 143–144, 1994.

[8] M. J. W. Hall, D.-A. Deckert, and H. M. Wiseman, “Quantum phenomena modeled by interactions between many classical worlds,” *Phys. Rev. X*, vol. 4, p. 041013, Oct 2014.

[9] P. Holland, “Computing the wavefunction from trajectories: particle and wave pictures in quantum mechanics and their relation,” *Annals of Physics*, vol. 315, no. 2, pp. 505 – 531, 2005.

[10] J. Schiff and B. Poirier, “Communication: Quantum mechanics without wavefunctions,” *The Journal of Chemical Physics*, vol. 136, no. 3, pp. –, 2012.

[11] D. Bohm, “A suggested interpretation of the quantum theory in terms of “hidden” variables. i,” *Physical Review*, vol. 85, no. 2, p. 166, 1952.

[12] D. Bohm, “A suggested interpretation of the quantum theory in terms of “hidden” variables.

ii,” *Physical Review*, vol. 85, no. 2, p. 180, 1952.

- [13] S. van der Walt, S. C. Colbert, and G. Varoquaux, “The numpy array: A structure for efficient numerical computation,” *Computing in Science & Engineering*, vol. 13, no. 2, pp. 22–30, 2011.
- [14] E. Jones, T. Oliphant, P. Peterson, *et al.*, “SciPy: Open source scientific tools for Python,” 2001–. [Online; accessed 2017-05-11].
- [15] M. Pillai, J. Goglio, and T. G. Walker, “Matrix numerov method for solving schrödinger’s equation,” *American Journal of Physics*, vol. 80, no. 11, pp. 1017–1019, 2012.
- [16] S. J. Sheather, “Density estimation,” *Statist. Sci.*, vol. 19, pp. 588–597, 11 2004.
- [17] R. Bell, *The tunnel effect in chemistry*. 1980.
- [18] I. W. McKeague, E. A. Peköz, and Y. Swan, “Stein’s method, many interacting worlds and quantum mechanics,” 2016.
- [19] K. R. Stromberg and A. M. Society, *An introduction to classical real analysis*. Wadsworth International Group Belmont, California, 1981.
- [20] A. Mohebbi and M. Dehghan, “The use of compact boundary value method for the solution of two-dimensional schrödinger equation,” *Journal of Computational and Applied Mathematics*, vol. 225, no. 1, pp. 124 – 134, 2009.

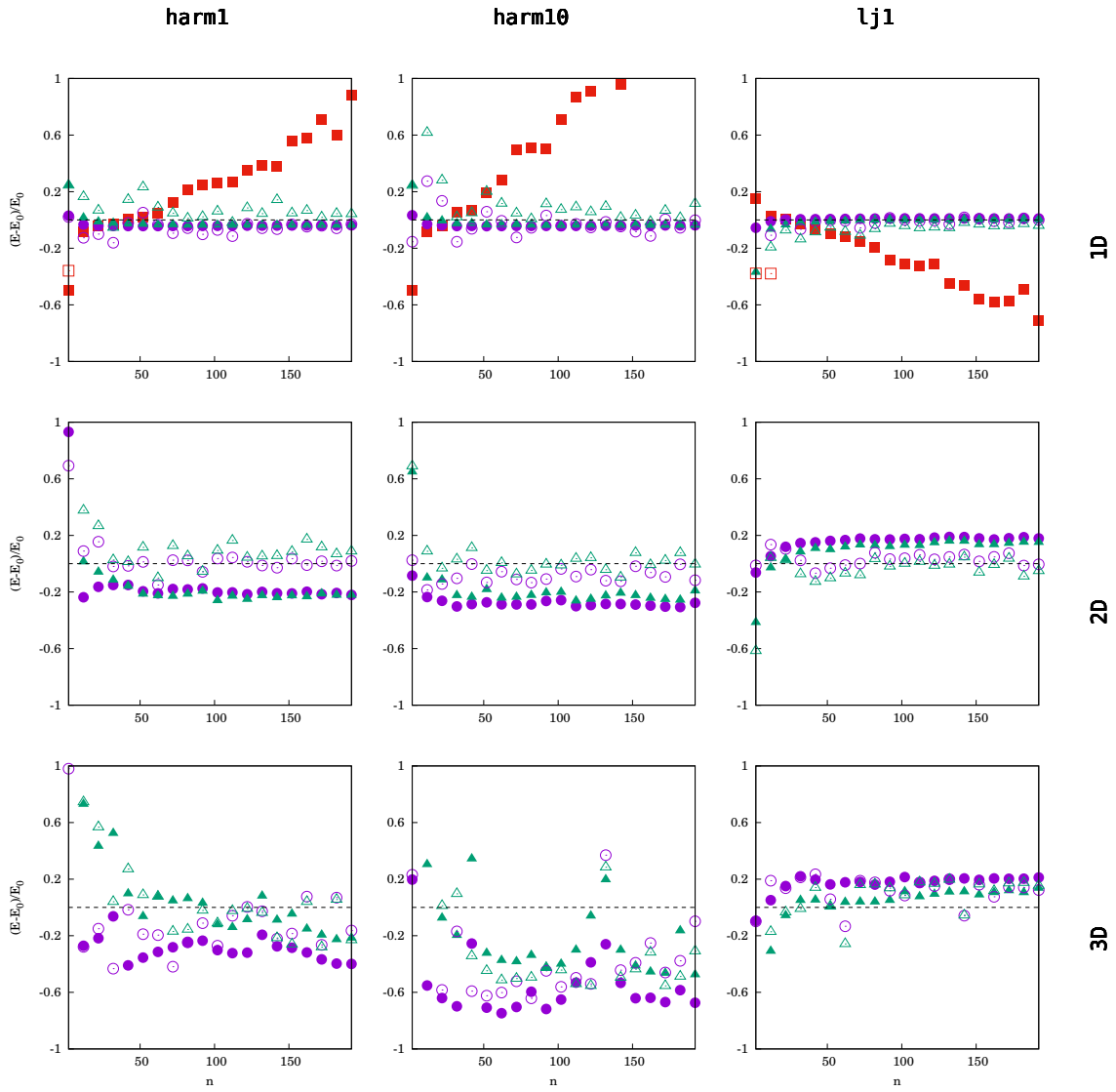


FIG. 2. MIW energy error with an ideal distribution vs. number of worlds plotted for various potentials and dimensionalities. Ideal energies were computed with a matrix Numerov algorithm using grids of 200, 40 and 15 points of side respectively for 1, 2 and 3D. Circles represent the Gaussian kernel, triangles the exponential one, and squares the method from the original paper (only applicable to 1D). Filled dots represent uniformly distributed particles, empty ones the Monte-Carlo distributed ones

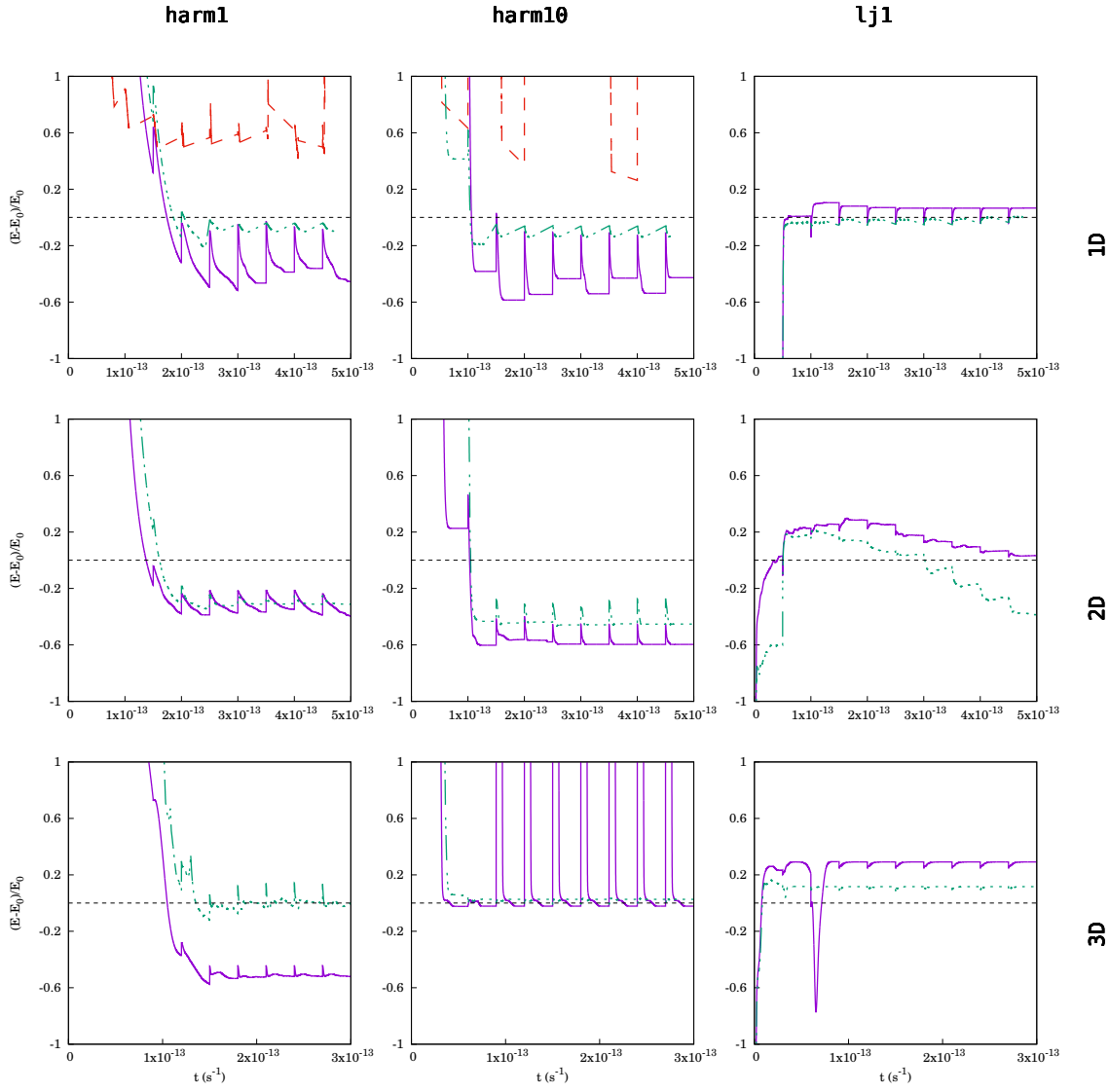


FIG. 3. Energy convergence during the relaxation process for different potentials and dimensionalities. Continuous lines represent the Gaussian kernel, dot-dashed lines the exponential one, and dashed lines the method from [8].

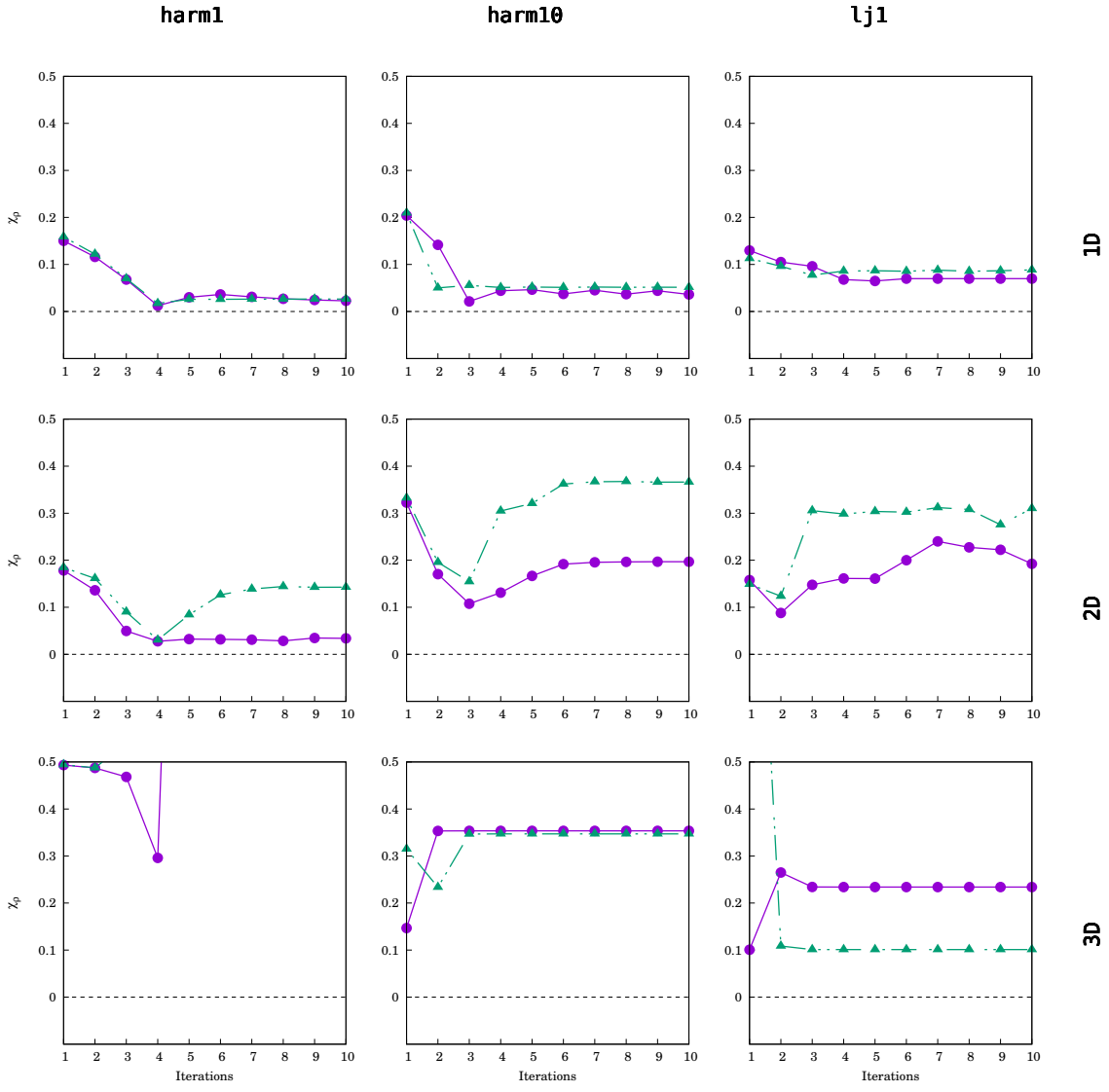


FIG. 4. Ground state density error RSS convergence during the relaxation process for different potentials and dimensionalities. Circles represent the Gaussian kernel and triangles the exponential one. It was not possible to compute the quantity for the original method as it does not provide a continuous approximation for the density.

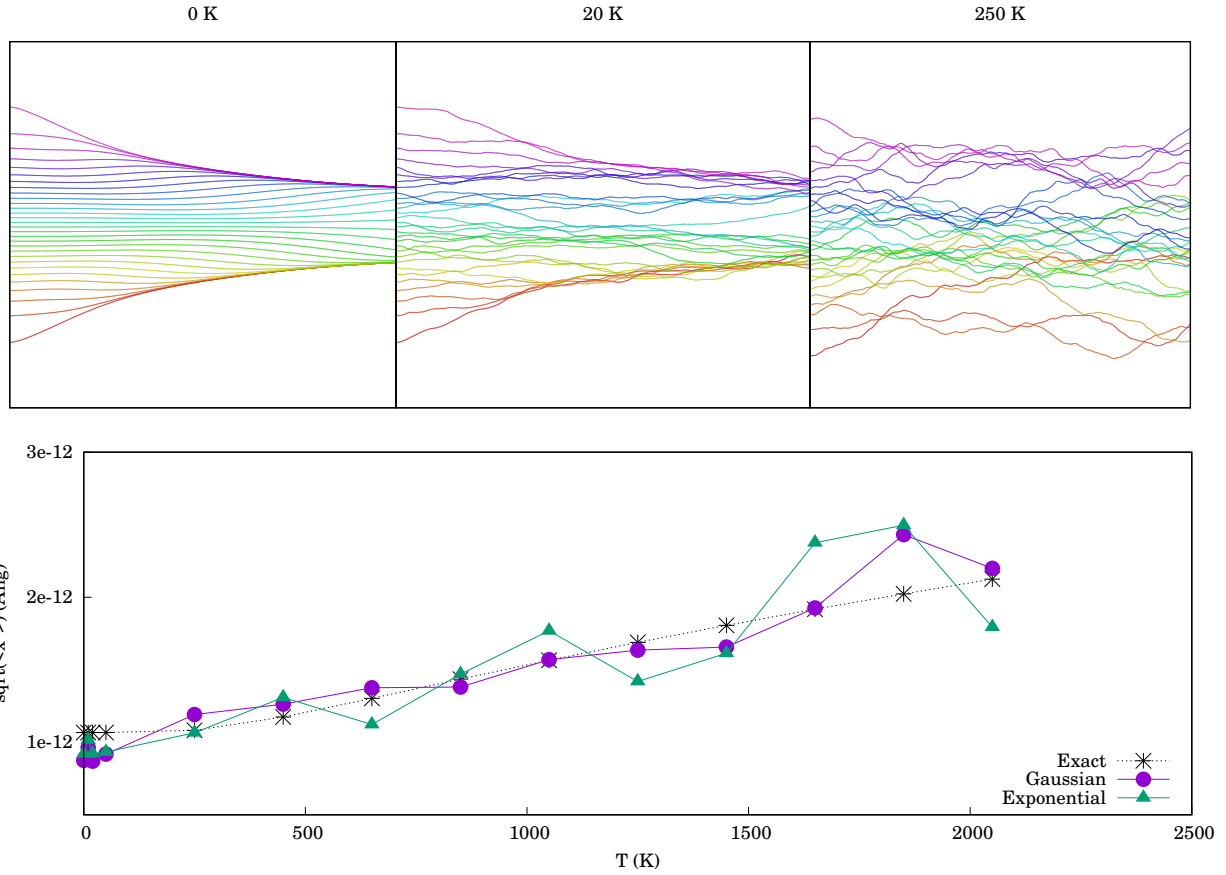


FIG. 5. Quantum trajectories at different temperatures and computed value of $\sqrt{\langle x^2 \rangle}$ up to 2000 K for a particle in a harmonic oscillator with $k = 1\text{ eV}/\text{\AA}^2$, using $N = 30$ MIW worlds.

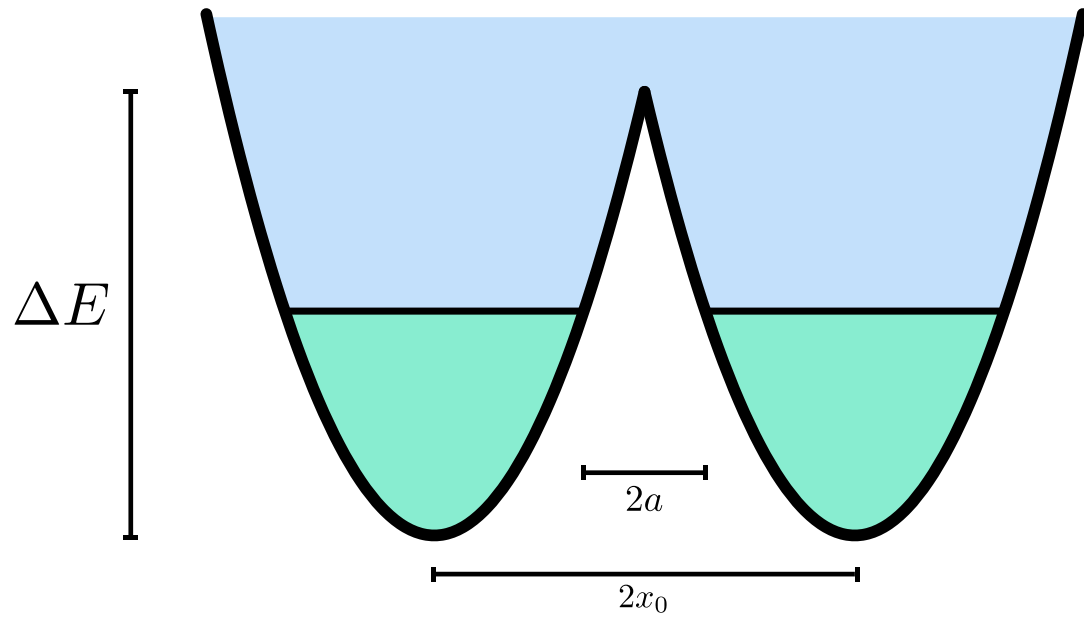


FIG. 6. Double harmonic well potential as described by R.P. Bell in [17]. The barrier height is ΔE , x_0 is the distance of the minimum from the barrier and a is the distance of the turning point - namely, the point where the potential exceeds the zero point energy of the particle.

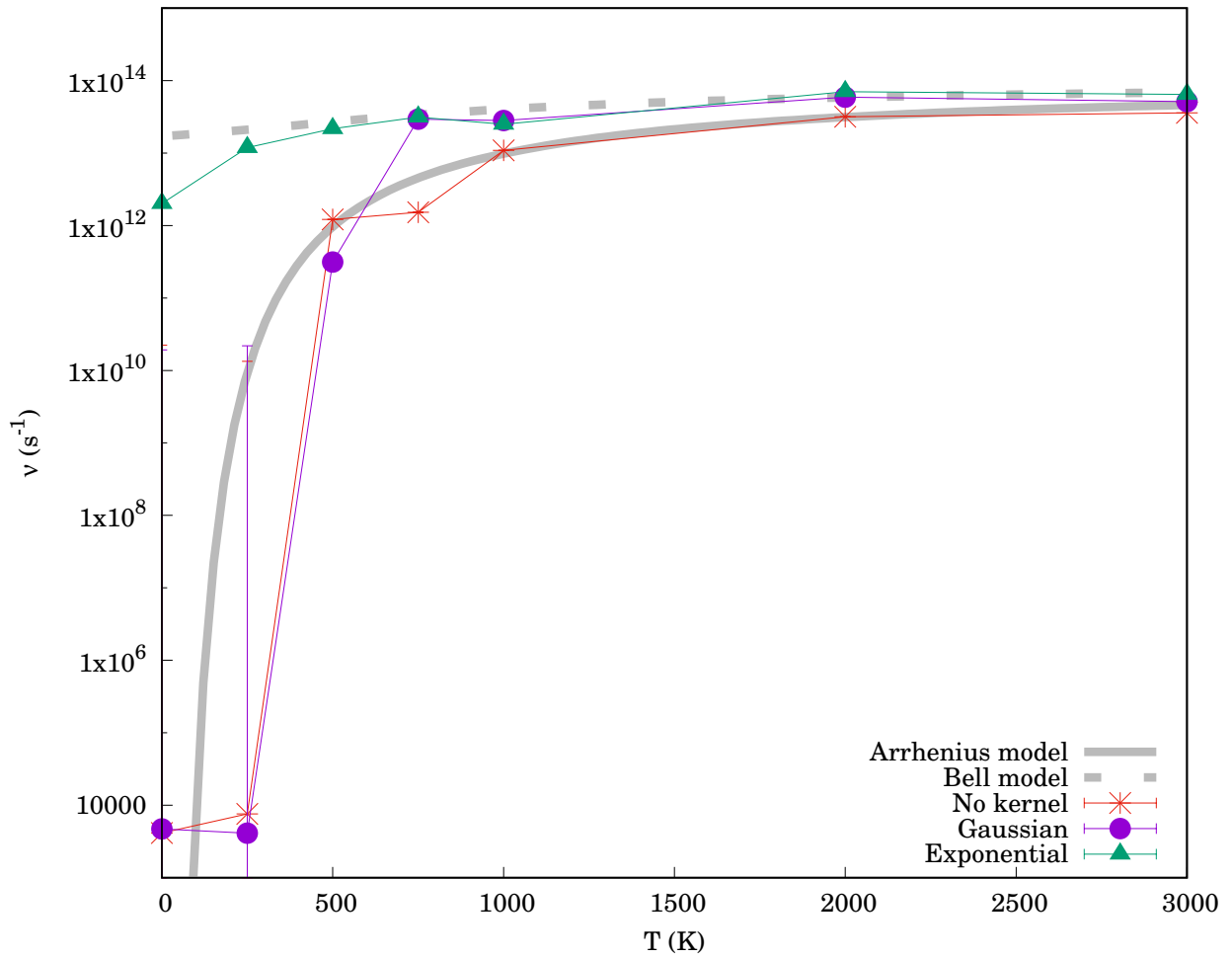


FIG. 7. Jumping rates in a MIW simulation on a double harmonic well potential. The fitted parameters are shown with error bars (though most of them are so small as to be invisible) and overlapped with the Arrhenius and Bell models.